magnetochemistry

MDPI

Article

Fabrication of Dy_2O_3 Transparent Ceramics by Vacuum Sintering Using Precipitated Powders

Dianjun Hu [1,2], Xin Liu [1,2], Ziyu Liu [1,2], Xiaoying Li [1,2], Feng Tian [1,2], Danyang Zhu [1,2], Zhaoxiang Yang [1], Lexiang Wu [1] and Jiang Li [1,2,*]

[1] Key Laboratory of Transparent Opto-functional Inorganic Materials, Shanghai Institute of Ceramics, Chinese Academy of Sciences, Shanghai 201899, China; hudianjun@student.sic.ac.cn (D.H.); liuxin@student.sic.ac.cn (X.L.); liuziyu@student.sic.ac.cn (Z.L.); lixiaoying19@mails.ucas.ac.cn (X.L.); tianfeng@student.sic.ac.cn (F.T.); zhudanyang@student.sic.ac.cn (D.Z.); yangzx@mail.sic.ac.cn (Z.Y.); wulexiang@mail.sic.ac.cn (L.W.)

[2] Center of Materials Science and Optoelectronics Engineering, University of Chinese Academy of Sciences, Beijing 100049, China

* Correspondence: lijiang@mail.sic.ac.cn; Tel.: +86-21-69163689; Fax: +86-21-69906700

Abstract: As a kind of promising material for a Faraday isolator used in the visible and near infrared range, Dy_2O_3 transparent ceramics were prepared by vacuum sintering from the nano-powders synthesized by the liquid precipitation method using ammonium hydrogen carbonate as precipitant with no sintering aids. The synthesized precursor was calcinated at 950 °C–1150 °C for 4 h in air. The influences of the calcination temperature on the morphologies and phase composition of Dy_2O_3 powders were characterized. It is found that the Dy_2O_3 powder calcinated at 1000 °C for 4 h is superior for the fabrication of Dy_2O_3 ceramics. The Dy_2O_3 transparent ceramic sample prepared by vacuum sintering at 1850 °C for 10 h, and subsequently with air annealing at 1400 °C for 10 h, from the 1000 °C-calcined Dy_2O_3 powders, presents the best optical quality. The values of in-line transmittance of the optimal ceramic specimen with the thickness of 1.0 mm are 75.3% at 2000 nm and 67.9% at 633 nm. The Verdet constant of Dy_2O_3 ceramics was measured to be -325.3 ± 1.9 rad/(T·m) at 633 nm, about 2.4 times larger than that of TGG ($Tb_3Ga_5O_{12}$) single crystals.

Keywords: Dy_2O_3 transparent ceramics; liquid precipitation method; calcination temperature; isostatic pressing; vacuum sintering; Verdet constant

Citation: Hu, D.; Liu, X.; Liu, Z.; Li, X.; Tian, F.; Zhu, D.; Yang, Z.; Wu, L.; Li, J. Fabrication of Dy_2O_3 Transparent Ceramics by Vacuum Sintering Using Precipitated Powders. *Magnetochemistry* **2021**, *7*, 6. https://dx.doi.org/10.3390/magnetochemistry7010006

Received: 1 December 2020
Accepted: 19 December 2020
Published: 28 December 2020

1. Introduction

Along with the propelling of magneto-optical devices, it becomes gradually essential to investigate the state-of-the art technology to obtain magneto-optical materials due to their irreplaceable roles in laser [1], optical communication [2], optical fiber sensing [3], and other fields. The most widely studied and applied magneto-optical device is the magneto-optical isolator. The magneto-optical isolator is also known as an optical unidirectional passive device with the nonreciprocal optical transmission. Its main function is to prevent the beam reflecting from the optical fiber and components of the optical path from reentering the lasers, and avoid causing damage to its components or interference with the incident light [4,5]. The additional optical reflection will make the optical communication system unstable and thus limits the transmission of the long-distance optical signal. Therefore, the optical isolator, which only allows the optical signal to transmit in one direction along the optical path, is necessary to solve this problem.

Figure 1 shows the graphic representation of the Faraday effect; it shows that when a beam of polarized light passes through the magneto-optical materials (located in the magnetic field), along the direction of the magnetic field, the polarization plane of the transmitted light will deflect at a certain angle compared to the incident one. The deflection of the polarization plane caused by the Faraday effect has nothing to do with the direction

of light propagation, only with the direction of magnetic field [6,7]. This nonreciprocity of magneto-optical materials can effectively realize the isolation and modulation of optical signals, making them receive great attention and development [8]. The magneto-optical medium plays a key role in the isolator, so a suitable magneto-optical material is an important factor to promote the development of a Faraday isolator. At present, a lot of widely used magneto-optical materials have been reported, such as YIG ($Y_3Fe_5O_{12}$) [9–11], TGG ($Tb_3Ga_5O_{12}$) [12–14], and TAG ($Tb_3Al_5O_{12}$) [15–19]. It is known that Ce^{3+}, Pr^{3+}, Dy^{3+}, Ho^{3+}, and Tb^{3+} ions have excellent magneto-optical properties [20] due to their 4f–5d transition. Rare earth sesquioxides, Tb_2O_3 [21–24], Dy_2O_3 [25–28], and Ho_2O_3 [29–32], with a high concentration of rare earth ions, have a better prospect in the application of optical isolators, as their Verdet constant values are 3.8, 2.2, and 1.3 times higher than that of TGG single crystals, respectively [33]. Among these materials, Dy_2O_3 has several transparency windows in the visible 500–730 nm, near-IR (infrared) 1900–2300 nm, and mid-IR 3500–7500 nm ranges [27], making it promising for Faraday devices used in the visible range and near 2 μm.

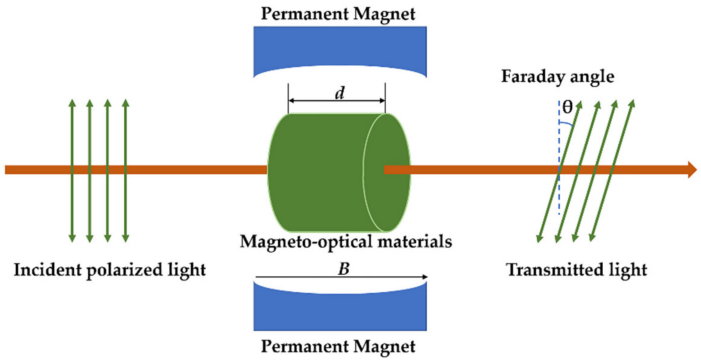

Figure 1. The graphic representation of the Faraday effect.

Dy_2O_3 undergoes phase transitions at high temperatures below the melting point [34], which makes the preparation of a Dy_2O_3 single crystal troublesome, whereas Dy_2O_3 polycrystalline ceramics can be synthesized at relatively low temperatures, at which Dy_2O_3 keeps a cubic C-type structure. Extensive efforts have been made to fabricate Dy_2O_3 ceramics. Dy_2O_3 transparent ceramics were firstly reported in a patent in 2002 [26]. Then in 2011, Morale et al. [25] processed nanocrystalline Dy_2O_3 ceramics using current activated pressure assisted densification (CAPAD), and the measured Verdet constant was above 300 rad/(T·m) at 632.8 nm. A series of optical ceramics based on $(Dy_xY_{0.95-x}La_{0.05})_2O_3$ (x = 0.7, 0.85 and 0.9) were prepared by vacuum sintering with self-propagating high-temperature synthesis of submicron powders, and the dependence of the Verdet constant on the wavelength in the 400 nm–1940 nm range was measured in the report [27]. Additionally, the temperature dependences of the Verdet constant, and their approximations in the temperature range of 80 to 294 K and in the wavelength range of 405 to 1064 nm, with the <10% deviation from the experimental data, were reported in [35]. Slezák et al. [28] also measured the temperature and wavelength dependence of the Verdet constant of Dy_2O_3 transparent ceramics for the temperature ranging from cryogenic 20 K up to room temperature, 297 K, in the wavelength range starting from visible 0.6 μm up to mid-infrared 2.3 μm. Aung et al. [36] obtained optical grade Dy_2O_3 ceramics, with an optical loss less than 0.1%/cm, by a pre-sintering and hot isostatic pressing treatment using ZrO_2 as a sintering aid.

High-quality powder is the key to obtain high performance transparent ceramics. The particle size, shape, and agglomeration state of powder will directly affect the densification behavior and microstructure of ceramics. A good powder combined with a proper sintering schedule is conducive for the elimination of pores and the densification of ceramics. The liquid precipitation method has been explored as a method to effectively control the morphology of the powder. It can realize the synthesis of fine powders with uniform size

distribution and has been used for the preparation of various transparent ceramics, such as YAG($Y_3Al_5O_{12}$) [37], Lu_2O_3 [38], $MgAl_2O_4$ [39], and so on. However, to date, most of the efforts focused on Dy_2O_3 powders and ceramics have not been addressed using the liquid precipitation method.

In this paper, Dy_2O_3 transparent ceramics were fabricated by vacuum sintering from the precipitated nano-powders for the first time. Using NH_4HCO_3 (AHC) as precipitant and $(NH_4)_2SO_4$ as dispersant, the obtained precursor was calcinated at 950–1150 °C for 4 h in air. The influences of the calcination temperature on the morphologies, phase composition and the particle sizes of Dy_2O_3 powders were characterized. The microstructures of the Dy_2O_3 ceramics were identified. The optical and magneto-optical properties were also analyzed.

2. Materials and Methods

2.1. Materials

Dy_2O_3 (99.99%, Golden Dragon Rare-Earth Co., Ltd., Changting, China), HNO_3 (G3, Shanghai Aoban Technology Co., Ltd., Shanghai, China), NH_4HCO_3 (Analytical grade, Aladdin, Shanghai, China) and $(NH_4)_2SO_4$ (Analytical grade, Sinopharm Chemical Reagent Co., Ltd., Shanghai, China) were used as raw materials.

2.2. Methods

The positive strike precipitation method was utilized to synthesize the Dy_2O_3 nano-powders. $Dy(NO_3)_3$ solution was obtained by adding the Dy_2O_3 powder into a concentrated nitric acid with stirring and heating. After the powder was completely dissolved, the solution was diluted and then filtered to remove the insoluble impurities. The concentration of the $Dy(NO_3)_3$ solution determined by chemical analysis was 1.5076 mol/L. $(NH_4)_2SO_4$ was dissolved in deionized water as the dispersant with the concentration of 2.0 mol/L. AHC was dissolved in deionized water with a concentration of 2.0 mol/L as precipitant. Firstly, $(NH_4)_2SO_4$ solution was added to the metal ion solution with the molar ratio of Dy^{3+} to $(NH_4)_2SO_4$ being 1:1. Then the mixed solution was diluted with deionized water until 500 mL with the concentration of Dy^{3+} being 0.4 mol/L. Subsequently, the AHC solution was added into the mixed solution at a speed of 3 mL/min under fast-speed stirring at room temperature. In the process of precipitation, the pH of the metal ion solution increased from 1.3 to 6.7. After 400 mL of AHC solution was added, the precipitated products were aging for 4 h and then the precipitation was washed with deionized water and anhydrous ethanol several times. After drying at 70 °C for 36 h and sieving with a 200screen mesh, the precursor was obtained. Then the precursors were calcined at 950–1150 °C for 4 h in air, respectively. The obtained Dy_2O_3 powders were dry pressed and cold isostatic pressed to get green bodies. The pellets were then vacuum sintered at 1675, 1780, and 1850 °C for 10 h, and air annealed at 1400 °C for 10 h. Finally, the Dy_2O_3 ceramics were mirror polished on both sides with a thickness of 1.0 mm.

2.3. Characterization

The compositions of the precursor and the calcined Dy_2O_3 powders were investigated by the Fourier transform infrared spectrometer (FTIR, Bruker VERTEX 70 spectrophotometer, Ettlingen, Germany). The thermogravimetry and differential thermal analysis (TG-DTA) of the precursor were measured by the thermal analyzer (Thermoplus EVO II, Rigaku, Tokyo, Japan). The phases of the precursor and the calcined powders were identified by the X-ray diffraction (XRD, D8 ADVANCE, Bruker AXS GMBH, Karlsruhe, Germany) using Cu K_α radiation in the range of $2\theta = 20°–80°$. The specific surface area of the calcined Dy_2O_3 powders was performed by the Quadrasorb SI (Quantachrome Instruments, Boynton Beach, FL, USA) with N_2 as the absorption gas at 77 K. The morphology of the Dy_2O_3 powders was observed by the field emission scanning electron microscopy (FE-SEM, SU9000, Hitachi, Tokyo, Japan). The microstructures of the Dy_2O_3 ceramic specimens were investigated by a field emission scanning electron microscopy (FE-SEM, SU8220, Hitachi, Tokyo, Japan) and the optical microscopy (U-CMAD3, Olympus, Tokyo, Japan).

The in-line transmittance curves of the Dy_2O_3 ceramics with the thickness of 1.0 mm were measured by a UV-VIS-NIR (ultraviolet-visible-near infrared) spectrophotometer (Model Cray-5000, Varian, Palo Alto, CA, USA) in the wavelength range of 300 to 2200 nm. The Verdet constant was measured by the extinction method with an instrument consisting of a He-Ne laser (wavelength = 632.8 nm), an electromagnet and two polarizers at room temperature, as shown in Figure 2. Firstly, the magnetic field is not applied to the sample, and the position of the light transmission axis of the output polarizer is adjusted to make the transmission axis of the two polarizers in orthogonal, and the detected intensity of the transmitted light reaches the minimum, that is, extinction occurs. Then, after applying a certain magnetic field to the measured sample, the detected intensity of the transmitted light changes, indicating that the polarization plane of the light rotates when passing through the sample in the magnetic field. In order to reproduce the extinction phenomenon, the output polarizer needs to rotate a certain angle θ to make the detected intensity reach the minimum again, and the θ is the Faraday angle to be measured. The Verdet constant (V) can be calculated by the formula [40]:

$$\theta = VBd$$

where d is the thickness of the sample (d = 1.0 mm), B is the magnetic field strength, θ is the Faraday angle.

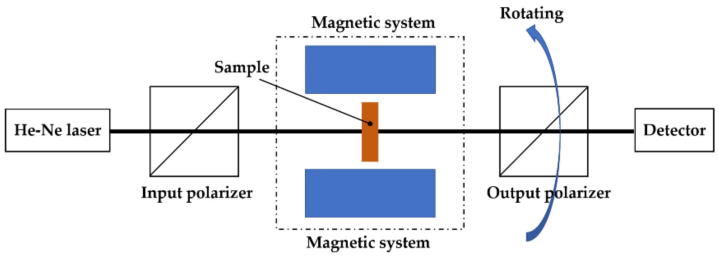

Figure 2. The schematic diagram for measuring the Verdet constant.

3. Results and Discussion

The Dy_2O_3 precursor prepared by liquid precipitation method needs to be calcined at a certain temperature to become Dy_2O_3 powder. The selection of the calcination temperature is extremely important for the preparation of high-quality nano-powder and transparent ceramics. Figure 3 shows the TG-DTA-DTG curves of the Dy_2O_3 precursor obtained from liquid precipitation method. The DTG curve results from the first derivative of the TG curve, from which the temperature range of each stage can be got clearly. There are four stages in the thermal decomposition of the precursor during the heating process, with a total weight loss of 41.9%. The first stage is from room temperature to about 155 °C, and the weight loss is 13.6%, which is mainly caused by the evaporation of absorbed water and residual ethanol, and the decomposition of partial crystallized water, and the endothermic peak located at about 73 °C is due to the release of ethanol. The weight loss of the second stage from 155 to 290 °C is 8.3%, which is attributed to the removal of ammonium radical, OH^-, and residual crystal water. The endothermic peak centered at about 253 °C is related to the removal of residual crystal water and the dehydration of OH^-. The weight loss of the third stage from 290 °C to 683 °C is 18.4%, which is attributed to the decomposition of carbonate and OH^-. The endothermic peak centered at about 486 °C is mainly ascribed to the decomposition of carbonate. The wide exothermic peak in the temperature range of 580 to 650 °C, with the center at 610 °C, is related to the formation of the Dy_2O_3. The 1.6% weight loss above 683 °C is related to the decomposition of the residual carbonates and sulfates.

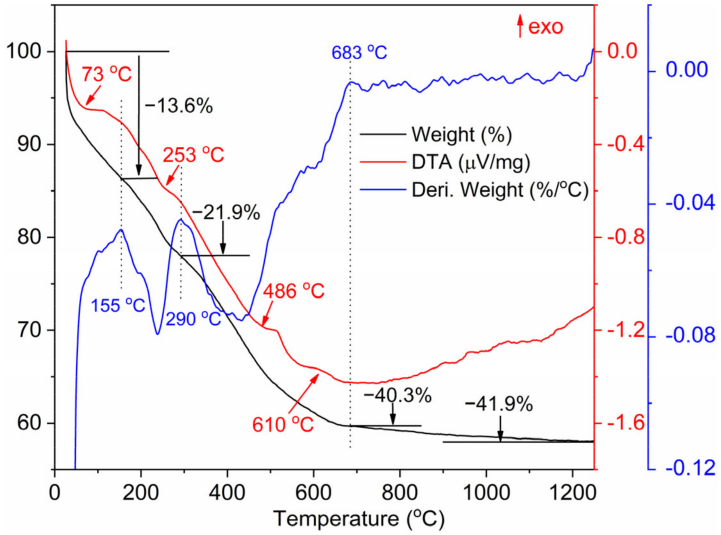

Figure 3. TG-DTA-DTG curves of the Dy_2O_3 precursor.

The thermal analysis of the precursor shows that the formation of Dy_2O_3 appeared at around 610 °C. In order to verify this conjecture, we calcined the Dy_2O_3 precursor at 600 and 650 °C for 1 h, respectively. Figure 4 shows the FTIR spectra of the Dy_2O_3 precursor and the powders calcined at different temperatures. The wide absorption band centered at about 3400 cm^{-1} and the 1635 cm^{-1} shoulder are corresponding to the bending and stretching vibrations of the O-H bond and the H-O-H bending mode of crystalline water, respectively [41,42]. These peaks at 1520, 1405, 1088, 844, 762, and 685 cm^{-1} are all ascribed to the existence of the CO_3^{2-}. Two absorption peaks at 1520 and 1405 cm^{-1} are attributed to ν_3 stretching mode of the C-O bond in CO_3^{2-} group [38]. These peaks at 1088, 844, 762, and 685 cm^{-1} are ascribed to the ν_1 symmetric stretch, δ out of plane bending vibration, ν_3 and ν_6 vibration of CO_3^{2-}, respectively [43]. Therefore, the precursor may be the dysprosium hydroxycarbonate with crystal water. For the powder calcined at 600 °C, the absorption peaks of O-H and CO_3^{2-} become weaker, and a new absorption peak of cubic Dy_2O_3 located at 555 cm^{-1} [44,45] appears, meaning that Dy_2O_3 has been generated at 600 °C. The absorption peaks of O-H and CO_3^{2-} still exist when the calcination temperature increases to 650 °C, indicating that the decomposition of the precursor is incomplete. Therefore, in order to obtain the pure Dy_2O_3 powders, the synthesized precursor was calcined above 650 °C. Figure 4 also presents the FTIR spectra of the Dy_2O_3 powders calcined at 950–1150 °C for 4 h, as can be seen that there are no obvious absorption peaks except that of the Dy_2O_3. Therefore, these Dy_2O_3 powders calcined at 950–1150 °C were chosen as raw materials for the fabrication of Dy_2O_3 transparent ceramics.

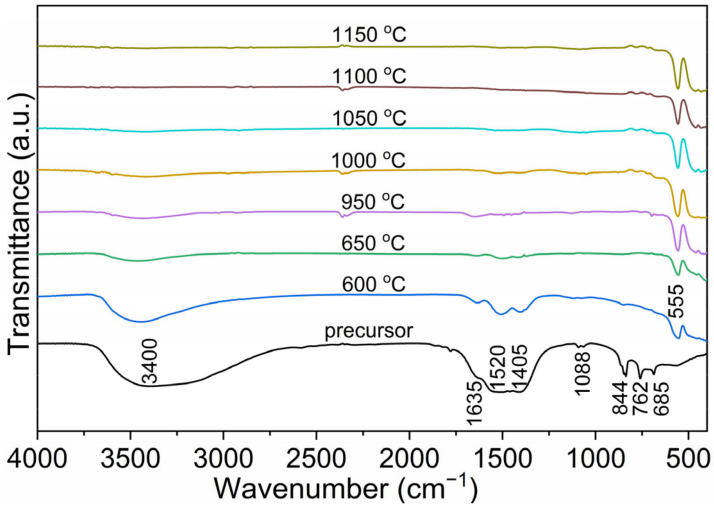

Figure 4. FTIR spectra of the Dy_2O_3 precursor and the powders calcined at 600, 650, and 950–1150 °C.

The XRD patterns of the Dy_2O_3 powders calcined at 600, 650, and 950–1150 °C are shown in Figure 5. All the characteristic diffraction peaks of the powders calcined at 600 and 650 °C correspond to the cubic dysprosium oxide phase (PDF#43-1006), meaning that the Dy_2O_3 phase has been generated at 600 °C, which is consistent with the result of FTIR, but slightly lower than the result of 610 °C in Figure 3 due to the hysteresis in the measurement of TG-DTA. Figure 5 also presents the XRD patterns of the precursor and the Dy_2O_3 powders calcined at 950–1150 °C for 4 h. It is noted that the crystallinity of the synthesized precursor is low. After calcination at 950–1150 °C, the diffraction peaks of obtained powders are consistent with the standard card of Dy_2O_3 (PDF#43-1006). These sharp diffraction peaks indicate the enhanced crystallinity of the powders. The average crystallite sizes (D_{XRD}) of the Dy_2O_3 powders are calculated by the Scherrer formula. The formula is as follows [46]:

$$D_{XRD} = 0.89\lambda/(\beta \cdot \cos\theta)$$

where λ is the wavelength of Cu K_α radiation, β is the full width at half maximum (FWHM) of a diffraction peak at Bragg angle θ. The calculated results of D_{XRD} are shown in Table 1. With the increase in the calcination temperature from 950 to 1150 °C, the D_{XRD} gradually increases from 79.6 to above 100 nm. The average particle size (D_{BET}) of Dy_2O_3 powder after calcination can be calculated by the following formula [47]:

$$D_{BET} = 6/(\rho \cdot S_{BET})$$

where ρ is the density of Dy_2O_3 (8.168 g/cm^3), S_{BET} is the specific surface area measured by the BET method. The S_{BET} and the calculated results of D_{BET} of Dy_2O_3 powders are also present in Table 1, and the values of D_{BET} are larger than those of D_{XRD}, indicating that these powders may be slightly agglomerated. The agglomeration degree of Dy_2O_3 nano-powder can be presented by the ratio of D_{BET} to D_{XRD}, the smaller value of ratio indicates the better dispersity [48]. For the Dy_2O_3 nano-powders calcined at different temperatures, the values of D_{BET}/D_{XRD} decrease firstly when the calcination temperature increases from 950 to 1000 °C. With the further increase in calcination temperature, the values increase gradually. The Dy_2O_3 nano-powder calcined at 1000 °C shows the smallest D_{BET}/D_{XRD}, indicating that the 1000 °C-calcined Dy_2O_3 nano-powder shows a good dispersion with a low agglomeration degree, which is conducive to the preparation of Dy_2O_3 transparent ceramics.

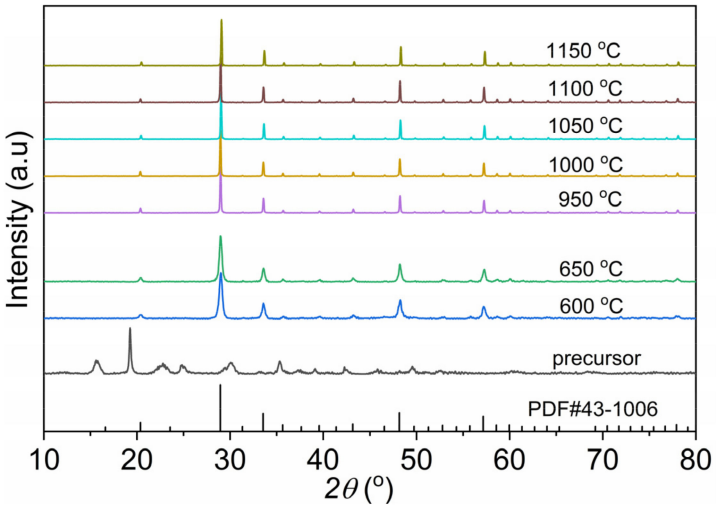

Figure 5. XRD patterns of the precursor and the Dy_2O_3 powders calcined at 600, 650, and 950–1150 °C.

Table 1. The specific surface areas (S_{BET}), average particle sizes (D_{BET}) and average crystallite sizes (D_{XRD}) of the Dy_2O_3 powders calcined at 950–1150 °C for 4 h.

Temperature (°C)	S_{BET} (m^2/g)	D_{BET} (nm)	D_{XRD} (nm)	D_{BET}/D_{XRD}
950	5.596	131.3	79.6 ± 1.2	1.65
1000	5.131	143.2	88.7 ± 2.2	1.61
1050	4.675	157.1	92.6 ± 1.5	1.70
1100	3.044	241.3	94.7 ± 1.4	2.55
1150	2.591	283.5	>100	-

Figure 6 shows the FE-SEM photographs of precursor and Dy_2O_3 powders calcined at 950–1150 °C for 4 h. The precursor shows a needle or flake shape with a loose structure. After calcining the precursor at 950–1150 °C for 4 h, the morphology of the powder changes greatly, forming clear and spherical like nanoparticles. It can be seen from Figure 6 that the calcination temperature has a significant effect on the particle size, morphology and agglomeration of the powder. When the calcination temperatures are orderly 1050, 1100, and 1150 °C, the powders have similar morphologies, and are composed of small near-spherical particles with weak agglomeration.

Using Dy_2O_3 powders calcined at 950–1150 °C for 4 h, Dy_2O_3 transparent ceramics were fabricated by vacuum sintering and then air annealing. The photograph of the Dy_2O_3 ceramics vacuum sintered at 1675, 1780, and 1850 °C for 10 h and air annealed at 1400 °C for 10 h is shown in Figure 7. The optical quality of Dy_2O_3 ceramics obtained from the powders calcined at different temperatures is obviously different at the same sintering temperature. The Dy_2O_3 ceramic samples fabricated from 950 °C-calcined powder appear translucent. It is noted that the Dy_2O_3 ceramic samples using the powders calcined at 1000 and 1050 °C exhibit relatively good transparency and the letters under them can be seen clearly. When the calcination temperature increases to 1100 and 1150 °C, the optical quality of the ceramics decreases obviously. The variation of optical quality for the Dy_2O_3 ceramic samples from powders calcined at different temperatures displays no significant difference under three different sintering schedules.

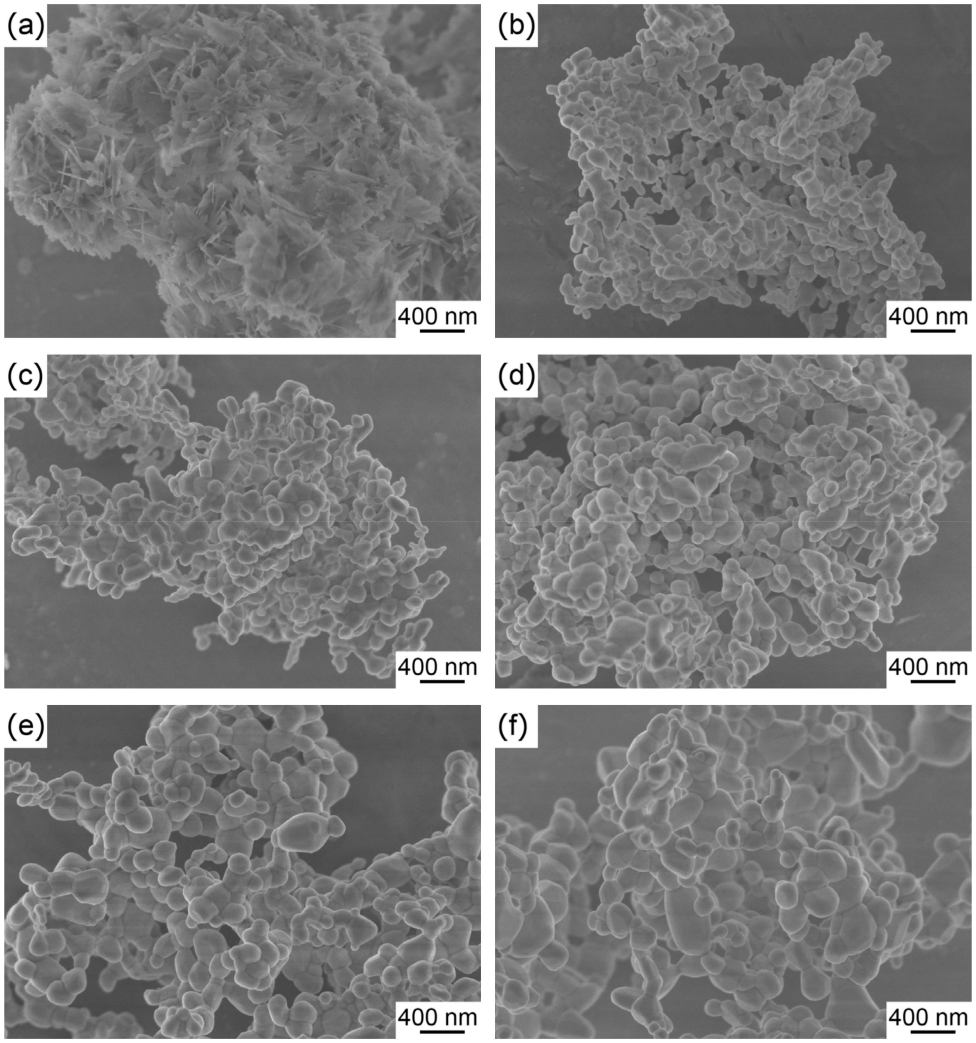

Figure 6. Field emission scanning electron microscopy (FE-SEM) pictures of the precursor (**a**) and the Dy_2O_3 powders calcined at different temperatures: (**b**) 950 °C, (**c**) 1000 °C, (**d**) 1050 °C, (**e**) 1100 °C, (**f**) 1150 °C.

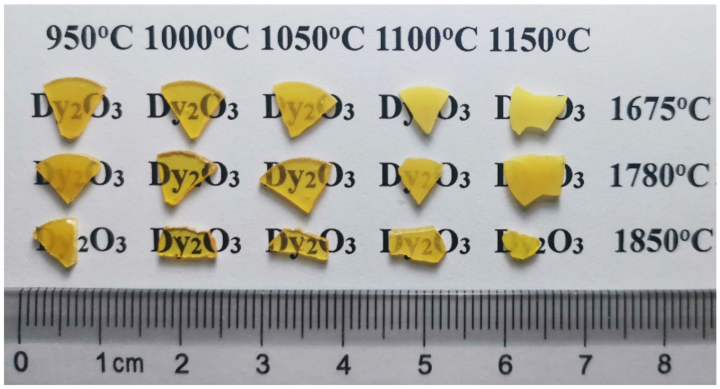

Figure 7. Photograph of the Dy_2O_3 ceramics vacuum sintered at 1675, 1780, and 1850 °C for 10 h and air annealed at 1400 °C for 10 h using Dy_2O_3 powders calcined 950–1150 °C for 4 h.

Figure 8a–c show the in-line transmittance curves of the corresponding Dy_2O_3 ceramic samples. With the increase in calcination temperature, the in-line transmittance of Dy_2O_3 ceramics firstly increases and then decreases. The Dy_2O_3 ceramic samples fabricated from 950 °C-calcined powder show low in-line transmittance, which is due to the incomplete grain growth observed from Figure 6b and weak agglomeration (D_{BET}/D_{XRD} = 1.65) of

Dy_2O_3 powder, and the weak agglomeration caused by the high specific surface energy (S_{BET} = 5.596 m^2/g) will lead to different grain boundary migration rate in the sintering process, being not conducive to densification. The ceramic samples with 1.0 mm thickness from 1000 °C-calcined Dy_2O_3 powder show the best transparency, and their in-line transmittances reach 69.2, 70.0, and 75.3% at 2000 nm, and 44.2, 56.8, and 67.9% at 633 nm, corresponding to the sintering temperature of 1675, 1780, and 1850 °C, respectively. The in-line transmittances of the samples decrease when the calcination temperature of Dy_2O_3 powder is further enhanced to 1050 °C. The slight decrease in the in-line transmittance is attributed to the increased agglomeration degree among primary particles (D_{BET}/D_{XRD} = 1.70), which reduces the sinterability of Dy_2O_3 powders. When the calcination temperature further increases to 1100 and 1150 °C, the in-line transmittance decreases greatly. For the powder calcined at high temperatures, there are sintering necks between particles (Figure 6e,f), increasing agglomeration degree and leaving poor sintering activity [13,49]. Therefore, the Dy_2O_3 powder calcined at 1000 °C is the most suitable for the fabrication of Dy_2O_3 transparent ceramics.

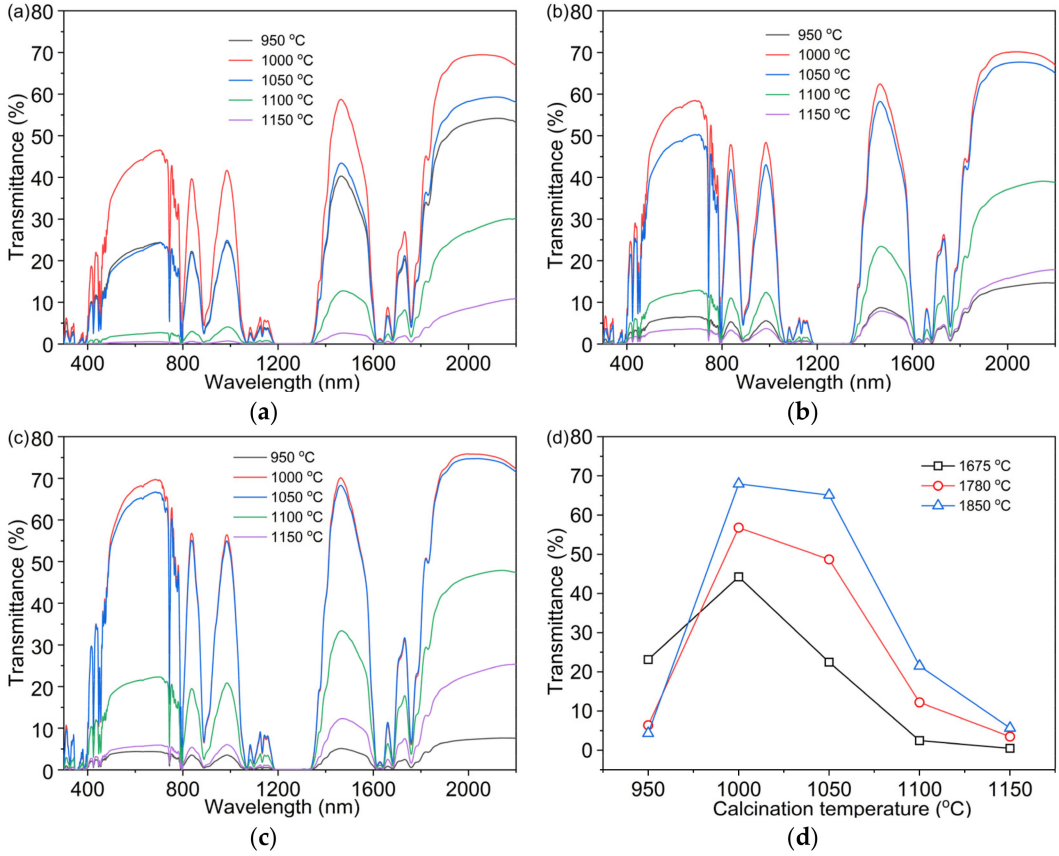

Figure 8. In-line transmittance curves of the Dy_2O_3 ceramics sintered at 1675 °C (**a**), 1780 °C (**b**) and 1850 °C (**c**) for 10 h followed by air annealing at 1400 °C for 10 h using the powders calcined at 950–1150 °C for 4 h and (**d**) the values of in-line transmittance at 633 nm versus calcination temperature for Dy_2O_3 powders (thickness = 1.0 mm).

Figure 9 shows the optical microscopy and FE-SEM pictures of the thermally-etched and the fracture surfaces of the Dy_2O_3 ceramics after vacuum sintering at different temperatures and air annealing at 1400 °C for 10 h from the 1000 °C-calcined Dy_2O_3 powder. Figure 9a,b present the surface and fracture microstructure of 1675 °C sintered Dy_2O_3 ceramics. The 1675 °C sintered specimen consists of uniform grains and has a nearly pore-free microstructure, and the statistical value of average grain size measured by the linear intercept method is about 25.6 μm. Figure 9b shows the transgranular fracture of Dy_2O_3 ceramics. With the temperature of vacuum sintering increasing, to 1780 and 1850 °C,

the grain size increases obviously, as shown in Figure 9c,e, respectively. From Figure 9d,f, it is known that the Dy_2O_3 ceramic samples are all transgranular fractures.

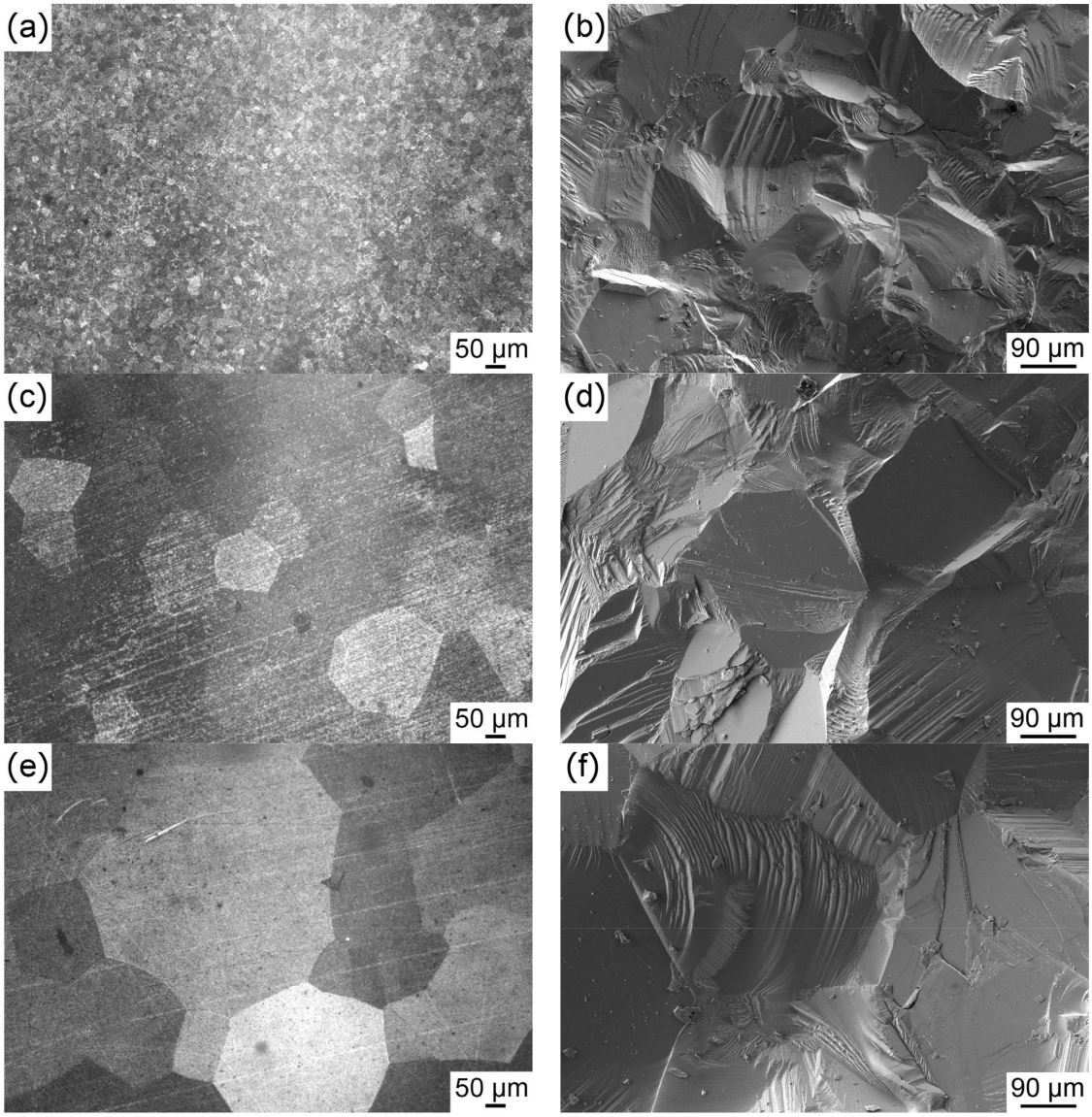

Figure 9. Optical microscopy (**a**,**c**,**e**) and FE-SEM pictures (**b**,**d**,**f**) of Dy_2O_3 ceramics sintered at different temperatures for 10 h and air annealed at 1400 °C for 10 h: (**a**) 1675 °C etching surface, (**b**)1675 °C fracture surface, (**c**) 1780 °C etching surface; (**d**) 1780 °C fracture surface, (**e**) 1850 °C etching surface; (**f**) 1850 °C fracture surface.

The Verdet constant is a key parameter for magneto-materials and it can reflect the deflection ability of the magneto-optical medium to polarized beam. The Verdet constant of 1675, 1780, and 1850 °C sintered Dy_2O_3 ceramics from 1000 °C calcined powders at 633 nm was measured to be about -324.8 ± 1.4 rad/(T·m), -325.3 ± 3.5 rad/(T·m) and -325.3 ± 1.9 rad/(T·m), respectively, about 2.4 times larger than that of the commercial TGG single crystal ($V_{TGG} = -135.8$ rad/(T·m) from [50]). Additionally, the measured results also show that the Verdet constants of Dy_2O_3 ceramic samples are almost independent of their optical quality. Considering that Dy_2O_3 ceramics have high transmission and large Verdet constant at visible range and near 2 μm, this material is an important candidate for a Faraday isolator used in visible or 2 μm lasers.

4. Conclusions

Dy_2O_3 nano-powders were synthesized by the liquid precipitation method using AHC as precipitant. Dy_2O_3 phase appears at 600 °C during the decomposition period of precursor. The near-spherical nano-powder calcined at 1000 °C shows the best sintering activity, and has the average particle size of 143.2 nm. With the calcination temperature of the powder increasing from 950 °C to 1150 °C, the optical quality of Dy_2O_3 ceramics increases firstly and then decreases. The Dy_2O_3 ceramics from 1000 °C calcined powder shows the best optical quality. The optimal Dy_2O_3 ceramics were fabricated by vacuum sintering at 1800 °C for 10 h and air annealing at 1400 °C for 10 h. The in-line transmittance values of the optimal ceramic sample with 1.0 mm thickness are 75.3% at 2000 nm and 67.9% at 633 nm. The Verdet constant of Dy_2O_3 ceramics was measured to be about -325.3 ± 1.9 rad/(T·m) at 633 nm, 2.4 times larger than that of the commercial TGG single crystal. The large Verdet constant and high optical quality make Dy_2O_3 transparent ceramics promising for a Faraday isolator used in visible and 2 μm range.

Author Contributions: Conceptualization, methodology and software, D.H.; validation, X.L. (Xiaoying Li); formal analysis, Z.L.; investigation, D.H. and F.T.; resources, J.L. and L.W.; data curation, D.H. and X.L. (Xin Liu); writing—original draft preparation and writing—review and editing, D.H. and D.Z.; visualization, Z.Y. and L.W.; supervision, project administration and funding acquisition, J.L. All authors have read and agreed to the published version of the manuscript.

Funding: This research received no external funding.

Data Availability Statement: The data presented in this study are available in this article.

Acknowledgments: This research was funded by National Key R and D Program of China (Grant No. 2017YFB0310500), the Special Exchange Program of Chinese Academy of Sciences (Plan B), the key research project of the frontier science of the Chinese Academy of Sciences (No. QYZDB-SSW-JSC022).

Conflicts of Interest: The authors declare no conflict of interest.

References

1. Vojna, D.; Slezák, O.; Lucianetti, A.; Mocek, T. Verdet constant of magneto-active materials developed for high-power Faraday devices. *Appl. Sci.* **2019**, *9*, 3160. [CrossRef]
2. Dötsch, H.; Bahlmann, N.; Zhuromskyy, O.; Hammer, M.; Wilkens, L.; Gerhardt, R.; Hertel, P.; Popkov, A. Applications of magneto-optical waveguides in integrated optics: Review. *J. Opt. Soc. Am. B* **2005**, *22*, 240–253. [CrossRef]
3. Kumari, S.; Chakraborty, S. Study of different magneto-optic materials for current sensing applications. *J. Sens. Sens. Syst.* **2018**, *7*, 421–431. [CrossRef]
4. Shintaku, T. Integrated optical isolator based on efficient nonreciprocal radiation mode conversion. *Appl. Phys. Lett.* **1998**, *73*, 1946–1948. [CrossRef]
5. Bahlmann, N.; Lohmeyer, M.; Zhuromskyy, O.; Dötsch, H.; Hertel, P. Nonreciprocal coupled waveguides for integrated optical isolators and circulators for TM-modes. *Opt. Commun.* **1999**, *161*, 330–337. [CrossRef]
6. Freiser, M. A survey of magnetooptic effects. *IEEE Trans. Magn.* **1968**, *4*, 152–161. [CrossRef]
7. Pershan, P.S. Magneto-optical effects. *J. Appl. Phys.* **1967**, *38*, 1482–1490. [CrossRef]
8. Li, J.; Dai, J.W.; Pan, Y.B. Research progress on magneto-optical transparent ceramics. *J. Inorg. Mater.* **2018**, *33*, 1–8.
9. Wittekoek, S.; Robertson, J.M.; Popma, T.J.A.; Bongers, P.F. Faraday rotation and optical absorption of epitaxial films of $Y_{3-x}Bi_xFe_5O_{12}$. *AIP Conf. Proc.* **1973**, *10*, 1418–1422.
10. Ikesue, A.; Aung, Y.L. Development of optical grade polycrystalline YIG ceramics for faraday rotator. *J. Am. Ceram. Soc.* **2018**, *101*, 5120–5126. [CrossRef]
11. Aung, Y.L.; Ikesue, A.; Watanabe, T.; Makikawa, S.; Iwamoto, Y. Bi substituted YIG ceramics isolator for optical communication. *J. Alloy. Compd.* **2019**, *811*, 152059. [CrossRef]
12. Villaverde, A.B.; Donatti, D.A.; Bozinis, D.G. Terbium gallium garnet Verdet constant measurements with pulsed magnetic field. *J. Phys. C Solid State Phys.* **1978**, *11*, L495–L498. [CrossRef]
13. Li, X.Y.; Liu, Q.; Pan, H.M.; Jiang, N.; Yang, Z.X.; Xie, T.F.; Wu, L.X.; Li, J. Transparent $Tb_3Ga_5O_{12}$ magneto-optical ceramics sintered from co-precipitated nano-powders calcined at different temperatures. *Opt. Mater.* **2019**, *90*, 26–32. [CrossRef]
14. Li, X.Y.; Liu, Q.; Hu, Z.W.; Jiang, N.; Shi, Y.; Li, J. Influence of ammonium hydrogen carbonate to metal ions molar ratio on co-precipitated nanopowders for TGG transparent ceramics. *J. Inorg. Mater.* **2019**, *34*, 791–796. [CrossRef]
15. Aung, Y.L.; Ikesue, A. Development of optical grade $(Tb_xY_{1-x})_3Al_5O_{12}$ ceramics as Faraday rotator material. *J. Am. Ceram. Soc.* **2017**, *100*, 4081–4087. [CrossRef]

16. Lin, H.; Zhou, S.M.; Teng, H. Synthesis of $Tb_3Al_5O_{12}$ (TAG) transparent ceramics for potential magneto-optical applications. *Opt. Mater.* **2011**, *33*, 1833–1836. [CrossRef]
17. Dai, J.W.; Pan, Y.B.; Xie, T.F.; Kou, H.M.; Li, J. Highly transparent $Tb_3Al_5O_{12}$ magneto-optical ceramics sintered from co-precipitated powders with sintering aids. *Opt. Mater.* **2018**, *78*, 370–374. [CrossRef]
18. Liu, Q.; Li, X.Y.; Dai, J.W.; Yang, Z.X.; Xie, T.F.; Li, J. Fabrication and characterizations of $(Tb_{1-x}Pr_x)_3Al_5O_{12}$ magneto-optical ceramics for Faraday isolators. *Opt. Mater.* **2018**, *84*, 330–334. [CrossRef]
19. Rubinstein, C.B.; Van Uitert, L.G.; Grodkiewicz, W.H. Magneto-optical properties of rare earth (III) aluminum garnets. *J. Appl. Phys.* **1964**, *35*, 3069–3070. [CrossRef]
20. Berger, S.B.; Rubinstein, C.B.; Kurkjian, C.R.; Treptow, A.W. Faraday rotation of rare-earth (III) phosphate glasses. *Phys. Rev.* **1964**, *133*, A723–A727. [CrossRef]
21. Snetkov, I.; Permin, D.; Balabanov, S.S.; Palashov, O. Wavelength dependence of Verdet constant of Tb^{3+}:Y_2O_3 ceramics. *Appl. Phys. Lett.* **2016**, *108*, 161905. [CrossRef]
22. Ikesue, A.; Aung, Y.; Makikawa, S.; Yahagi, A. Polycrystalline $(Tb_xY_{1-x})_2O_3$ Faraday rotator. *Opt. Lett.* **2017**, *42*, 4399. [CrossRef]
23. Zhang, J.Y.; Chen, H.T.; Wang, J.P.; Wang, D.W.; Han, D.; Zhang, J.; Wang, S.W. Phase transformation process of Tb_2O_3 at elevated temperature. *Scr. Mater.* **2019**, *171*, 108–111. [CrossRef]
24. Ikesue, A.; Aung, Y.L.; Makikawa, S.; Yahagi, A. Total performance of magneto-optical ceramics with a bixbyite structure. *Materials* **2019**, *12*, 421. [CrossRef]
25. Morales, J.R.; Amos, N.; Khizroev, S.; Garay, J.E. Magneto-optical Faraday effect in nanocrystalline oxides. *J. Appl. Phys.* **2011**, *109*, 093110. [CrossRef]
26. Yagi, H.; Yanagitani, T. Translucent Rare Earth Oxide Sintered Article and Method for Production Thereof. EP patent EP20020743710, 24 June 2002.
27. Snetkov, I.L.; Yakovlev, A.I.; Permin, D.A.; Balabanov, S.S.; Palashov, O.V. Magneto-optical Faraday effect in dysprosium oxide (Dy_2O_3) based ceramics obtained by vacuum sintering. *Opt. Lett.* **2018**, *43*, 4041–4044. [CrossRef]
28. Slezák, O.; Yasuhara, R.; Vojna, D.; Furuse, H.; Lucianetti, A.; Mocek, T. Temperature-wavelength dependence of Verdet constant of Dy_2O_3 ceramics. *Opt. Mater. Express* **2019**, *9*, 2971–2981. [CrossRef]
29. Furuse, H.; Yasuhara, R. Magneto-optical characteristics of holmium oxide (Ho_2O_3) ceramics. *Opt. Mater. Express* **2017**, *7*, 827–833. [CrossRef]
30. Vojna, D.; Yasuhara, R.; Furuse, H.; Slezak, O.; Hutchinson, S.; Lucianetti, A.; Mocek, T.; Cech, M. Faraday effect measurements of holmium oxide (Ho_2O_3) ceramics-based magneto-optical materials. *High Power Laser Sci. Eng.* **2018**, *6*, E2. [CrossRef]
31. Balabanov, S.; Filofeev, S.; Ivanov, M.; Kaigorodov, A.; Kuznetsov, D.; Hu, D.J.; Li, J.; Palashov, O.; Permin, D.; Rostokina, E.; et al. Fabrication and characterizations of holmium oxide based magneto-optical ceramics. *Opt. Mater.* **2020**, *101*, 109741. [CrossRef]
32. Hu, D.J.; Li, X.Y.; Snetkov, I.; Yakovlev, A.; Balabanov, S.; Ivanov, M.; Liu, X.; Liu, Z.Y.; Tian, F.; Xie, T.F.; et al. Fabrication, microstructure and optical characterizations of holmium oxide (Ho_2O_3) transparent ceramics. *J. Eur. Ceram. Soc.* **2020**, *41*, 759–767. [CrossRef]
33. Dai, J.W.; Li, J. Promising magneto-optical ceramics for high power Faraday isolators. *Scr. Mater.* **2018**, *155*, 78–84. [CrossRef]
34. Zhang, Y.M.; Jung, I.-H. Critical evaluation of thermodynamic properties of rare earth sesquioxides (RE = La, Ce, Pr, Nd, Pm, Sm, Eu, Gd, Tb, Dy, Ho, Er, Tm, Yb, Lu, Sc and Y). *Calphad* **2017**, *58*, 169–203. [CrossRef]
35. Yakovlev, A.; Snetkov, I.; Permin, D.; Balabanov, S.; Palashov, O. Faraday rotation in cryogenically cooled dysprosium based (Dy_2O_3) ceramics. *Scr. Mater.* **2019**, *161*, 32–35. [CrossRef]
36. Aung, Y.L.; Ikesue, A.; Yasuhara, R.; Iwamoto, Y. Magneto-optical Dy_2O_3 ceramics with optical grade. *Opt. Lett.* **2020**, *45*, 4615–4617. [CrossRef]
37. Tian, F.; Chen, C.; Liu, Q.; Yavetskiy, R.; Ivanov, M.; Balabanov, S.; Feng, Y.G.; Liu, X.; Liu, Z.Y.; Hu, D.J.; et al. Optimizing co-precipitated Nd:YAG nanopowders for transparent ceramics. *Opt. Mater.* **2020**, *108*, 110427. [CrossRef]
38. Liu, Z.Y.; Toci, G.; Pirri, A.; Patrizi, B.; Feng, Y.G.; Wei, J.B.; Wu, F.; Yang, Z.X.; Vannini, M.; Li, J. Fabrication, microstructures, and optical properties of Yb:Lu_2O_3 laser ceramics from co-precipitated nano-powders. *J. Adv. Ceram.* **2020**, 9. [CrossRef]
39. Liu, Q.; Su, S.; Hu, Z.W.; Chen, X.P.; Xie, T.F.; Yang, Z.X.; Pan, H.M.; Liu, X.; Li, J. Fabrication and properties of Co:$MgAl_2O_4$ transparent ceramics for a saturable absorber from coprecipitated nanopowder. *J. Am. Ceram. Soc.* **2019**, *102*, 3097–3102. [CrossRef]
40. Yasuhara, R.; Tokita, S.; Kawanaka, J.; Kawashima, T.; Kan, H.; Yagi, H.; Nozawa, H.; Yanagitani, T.; Fujimoto, Y.; Yoshida, H.; et al. Cryogenic temperature characteristics of Verdet constant on terbium gallium garnet ceramics. *Opt. Express* **2007**, *15*, 11255–11261. [CrossRef]
41. Abu-Zied, B.M.; Asiri, A.M. Synthesis of Dy_2O_3 nanoparticles via hydroxide precipitation: Effect of calcination temperature. *J. Rare Earths* **2014**, *32*, 259–264. [CrossRef]
42. Dai, J.W.; Pan, Y.B.; Chen, H.H.; Xie, T.F.; Kou, H.M.; Li, J. Synthesis of Tb_4O_7 nanopowders by the carbonate-precipitation method for $Tb_3Al_5O_{12}$ magneto-optical ceramics. *Opt. Mater.* **2017**, *73*, 706–711. [CrossRef]
43. Salavati-Niasari, M.; Javidi, J.; Davar, F.; Fazl, A.A. Sonochemical synthesis of $Dy_2(CO_3)_3$ nanoparticles and their conversion to Dy_2O_3 and $Dy(OH)_3$: Effects of synthesis parameters. *J. Alloy. Compd.* **2010**, *503*, 500–506. [CrossRef]
44. Batsanov, S.S.; Grigor'eva, G.N.; Sokolova, N.P. Optical properties of oxides of the rare-earth metals. *J. Struct. Chem.* **1962**, *3*, 323–325. [CrossRef]

45. Ruchkin, E.D.; Sokolova, M.N.; Batsanov, S.S. Optical properties of oxides of the rare earth elements V. study of monoclinic modifications (B forms). *J. Struct. Chem.* **1968**, *8*, 410–414. [CrossRef]
46. Monshi, A.; Foroughi, M.R.; Monshi, M.R. Modified Scherrer equation to estimate more accurately nano-crystallite size using XRD. *World J. Nano Sci. Eng.* **2012**, *02*, 154–160. [CrossRef]
47. Li, S.S.; Liu, B.L.; Li, J.; Zhu, X.W.; Liu, W.B.; Pan, Y.B.; Guo, J.K. Synthesis of yttria nano-powders by the precipitation method: The influence of ammonium hydrogen carbonate to metal ions molar ratio and ammonium sulfate addition. *J. Alloy. Compd.* **2016**, *678*, 258–266. [CrossRef]
48. Chen, P.H.; Liu, Q.; Li, X.Y.; Feng, Y.G.; Chen, X.P.; Liu, X.; Wu, L.X.; Li, J. Influence of terminal pH value on co-precipitated nanopowders for yttria-stabilized ZrO_2 transparent ceramics. *Opt. Mater.* **2019**, *98*, 109475. [CrossRef]
49. Huang, X.Y.; Zhang, X.; Hu, Z.W.; Feng, Y.G.; Wei, J.B.; Liu, X.; Li, X.Y.; Chen, H.H.; Wu, L.X.; Pan, H.M.; et al. Fabrication of Y_2O_3 transparent ceramics by hot isostatic pressing from precipitated nanopowders. *Opt. Mater.* **2019**, *92*, 359–365. [CrossRef]
50. Snetkov, I.L.; Yasuhara, R.; Starobor, A.V.; Mironov, E.A.; Palashov, O.V. Thermo-optical and magneto-optical characteristics of terbium scandium aluminum garnet crystals. *IEEE J. Quantum Electron.* **2015**, *51*, 1–7. [CrossRef]